48th AIAA/ASME/SAE/ASEE Joint Propulsion Conference & Exhibit
30 July - 01 August 2012, Atlanta, Georgia

AIAA 2012-4024

Progress Towards a Miniaturized Electrospray Thruster for Propulsion of Small Spacecraft

S. Dandavino [*] , C. Ataman [†] , S. Chakraborty [‡] and H. Shea [§]
EPFL, Neuchatel, 2000, Switzerland
C. Ryan [¶] and J. Stark [‖]
Queen Mary University of London, London, E1 4NS, United Kingdom

Miniaturized electrical thrusters based on electrospray (or colloid) emitters could revolutionize the spacecraft industry by providing efficient propulsion capabilities to micro and nano satellites (1-100 kg). We report on our recent advances in the development of this technology within the MicroThrust (www.microthrust.eu) European consortium. We present the design and operation of the currently fabricated and next generation emitter arrays, describing their microfabrication process and measured performance. The emitters are out-of-plane internally fed capillaries micromachined in monolithic silicon. They are 100 μm tall and have an inner diameter of 5-10 μm. We operate the devices in both unipolar and bi-polar modes and find that the latest devices operate in a mixed regime, with the emitted spray a composition of ions and droplets. Their specific impulse is consequently in the few hundred seconds, highlighting the need for higher impedance, smaller emitters. Onset voltages are of than 800-850V for 200 μm inner diameter extractors, current levels for 19 emitter arrays of 2-3 μA. Preliminary analysis hints to plume half-angles of 35-40°, although these values depend on the operation mode and beam composition.

Nomenclature

g	Standard gravity (9.80665 m/s^2)
IL	Ionic Liquid
I_{sp}	Specific impulse, Seconds
I_T	Total emitted current, Amperes
q	Charge, Coulomb
m	Mass, kg
V_b	Beam potential, Volts

[*]PhD Student, Microsystems for Space Technologies Laboratory, simon.dandavino@epfl.ch, AIAA Student Member
[†]Post-doc, Microsystems for Space Technologies Laboratory, caglar.ataman@epfl.ch
[‡]PhD Student, Microsystems for Space Technologies Laboratory, subha.chakraborty@epfl.ch
[§]Associate Professor, Microsystems for Space Technologies Laboratory, herbert.shea@epfl.ch
[¶]Post-doc, School of Engineering and Materials Science, c.n.ryan@qmul.ac.uk
[‖]Professor, School of Engineering and Materials Science, j.p.w.stark@qmul.ac.uk

I. Introduction

Due to their high performance and relative simplicity, electrospray thrusters have long been acknowledged as a promising technology to provide propulsion capabilities to small spacecraft.[1] They use a conductive liquid propellant (often an ionic liquid), transported to an extraction site where they are subjected to a large electrical field applied by an annular electrode.

As the applied potential is increased, the liquid meniscus deforms into an increasingly sharp hyperboloid and eventually reaches an equilibrium between the field, its surface tension and internal pressure. The meniscus then has the shape of a Taylor cone,[2] with a tip radius in the order of 10^{-8} m. The local tip electric field in this configuration can reach values of order 10^9 V/m, even with relatively small voltages applied (0.5 - 1.5 kV), and drive the extraction of droplets, ions[3] or a combination of both from the liquid.

Ensuring the liquid transport by capillarity reduces considerably the footprint of the propulsion system by removing the need for pressurized tanks and lines, an advantage over competing electrical propulsion technologies. Capillary transport has been demonstrated for internally,[4–8] externally[9] or porously fed emitters.[10,11]

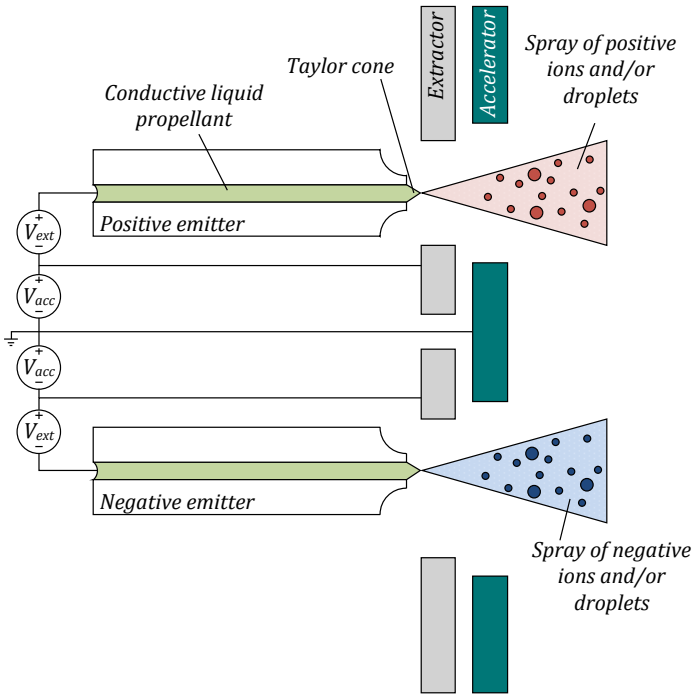

Figure 1. Operation of a bi-polar electrospray with extractor and accelerator stage.

Intrinsic to the technology is also the possibility to extract both positive and negative species, making it an electrical propulsion technology that does not require an external neutralizer.[12] Preliminary analysis, completed within the MicroThrust[a] project has shown that a complete system could be installed within a three-unit cubesat and carry it to lunar orbit.

Another key element of the technology is the potential to control the nature of the species emitted, from ion to droplet. These differ fundamentally in their charge over mass (q/m) ratio and consequently in their specific impulse (I_{sp}) vs thrust (T) characteristics, according to equations (1) and (2):

$$I_{sp} = \frac{1}{g}\sqrt{2V_b\frac{q}{m}} \tag{1}$$

$$T = I_T\sqrt{2V_b\frac{m}{q}} \tag{2}$$

where I_T is the total current of the emitted beam and V_b is the beam potential.

The extraction voltage having a major influence on the extraction process, the thrust and specify impulse can be adjusted by directly varying the potential on the extraction electrode. Adding an accelerator stage (not included in this work) can amplify both I_{sp} and thrust by increasing the beam potential V_b, resulting in a system only limited by the available power.

Our group has focused on internally fed emitters microfabricated in silicon (Figure 2). The internal feeding approach is advantageous has it affords a high level of propellant containment and reduced exposition to the space environment. It is also possible to accurately control the emitter tip geometry. This geometry is crucial as it will influence the local electric field and consequently the operation voltages. It also drives the key parameter of fluidic impedance. It has previously been shown that the nature of the emitted species is

[a] www.microthrust.eu

highly dependent on the liquid flow rate, such that the high specific impulse ionic mode of operation can be more easily achieved with very low flow rates.[13] In the past, we used silica microspheres to fill the emitters and therefore increase their hydraulic impedance.[13] This approach has now been discarded as it led to high variability in the filling configuration and effective impedance. Instead, the microfabrication methods are being improved to build smaller, higher aspect ratio emitters. This strategy is expected, in the short term, to yield devices that will not operate in ionic mode, but should, as the fabrication is optimized, to yield devices that operate repeatably in this mode.

In addition to allowing smaller dimension with higher precision, microfabrication permits the seamless manufacturing of large arrays of emitters operating in parallel, circumventing the I_{sp} vs T tradeoff. The small dimensions are also particularly adapted to small spacecraft applications. The currently fabricated thruster chips with wafer-level integrated extractor electrodes have an area of 10 x 10 mm^2 and are less than a mm thick.

This paper will summarize our recent advances on the development of the thruster chips. It will describe the latest generations of emitter designs, particularly with respect to the key parameter of hydraulic impedance. The microfabrication of the chips will be described, including the recently introduced wafer level bonding of the extractors. Finally, the performance of the thrusters will be presented following preliminary IV, time of flight and beam shape measurements.

II. Design

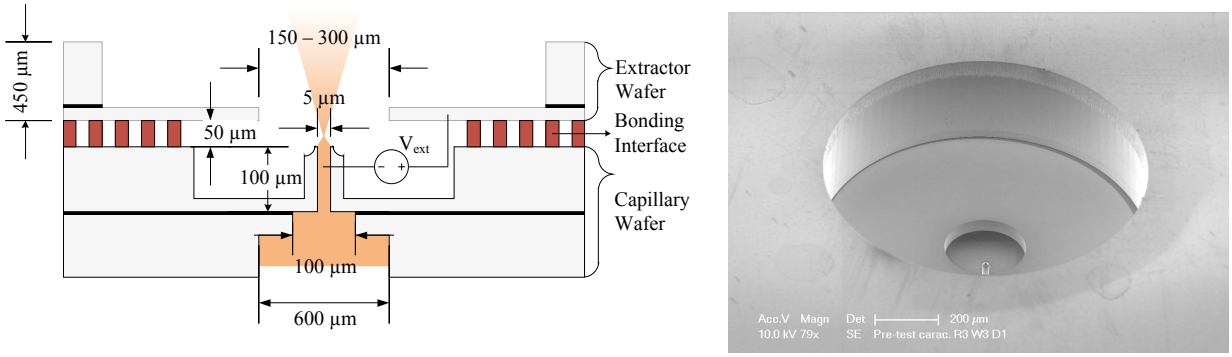

(a) (b)

Figure 2. Cross-section diagram (a) and SEM photo (b) of internally fed electrospray emitters.

Figure 2 shows a cross-section diagram of the microfabricated electrospray emitters. The capillaries are standing out of plane from the silicon bulk and fed with the ionic liquid $EMI - BF_4$ from their backside. They are $100\mu m$ tall and have an inner diameter ranging from 5 to 10 μm. Their edge is sharpened with an isotropic silicon etch to reduce the influence of the conductive silicon capillary on the field reaching the liquid cone and increase liquid containment (Figure 3). The extractor electrodes are placed 15 to 50 μm above the emitter tip and have an inner diameter ranging from 150 to 300 μm. Both the capillaries and extractors are fabricated separately and assembled at wafer level.

In operation, a positive or negative potential is applied to the liquid while the extractor level is grounded.

II.A. Hydraulic impedance

Hydraulic impedance plays a key role in the operation mode of the thrusters. Having a low flow rate (high impedance) is crucial for accessing the high I_{sp} ionic mode so that increasing the impedance has for some time been the subject of considerable development efforts. The present limitations lie with the microfabrication process, which limits the aspect ratio of the etch that defines the capillary interior. As mentioned earlier, earlier generations of the emitters used a process of silica microbead filling and silanization as a workaround to effectively reduce the inner diameter of the capillary (Figure 4).

To quantify this reduction, we use, as Lenguito,[6] a model adapted from Ergun[14] to compute the effective inner diameter D_{eff} of the emitter (Equation 3),

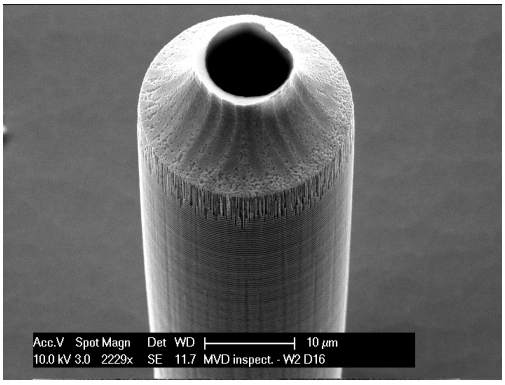

(a)

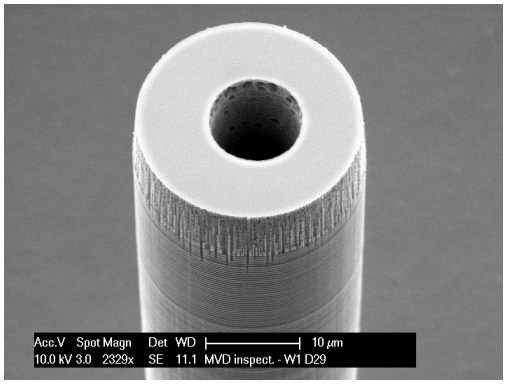

(b)

Figure 3. SEM closeups of sharpened (a) and unsharpened (b) emitter tips.

$$D_{eff} = \sqrt[4]{\frac{16}{75}\frac{D_s^2 D^2 \epsilon^3}{(1-\epsilon)^2}} \tag{3}$$

where D_s is the diameter of the microspheres, D is the inner diameter of the capillary and ϵ is the void fraction. The hydraulic impedance R_{fl} is then computed from the well-known Hagen-Poiseuille equation:

$$R_{fl} = \frac{128\mu L}{\pi D_{eff}^4} \tag{4}$$

where μ is the dynamic viscosity of the fluid (0.038 $Pa \cdot s$ for $EMI - BF_4$[15]), L is the length of the capillary and D_{eff} its inner diameter.

Table 1 gives a summary of the inner diameter of the fabricated first and second generation emitters, including the estimation of the effective inner diameter due to the bead filling. The estimation of minimum and maximum values for the inner diameter of the bead filled emitters were done by using a void fraction ranging from 0.25 to 0.65. Given the observed variation in the filling arrangement, and based on other work,[16–18] this was felt to be a reasonable assumption. The resulting estimated effective hydraulic impedance varied by nearly 1000%, indicating that different emitters, even within a single chip, could have significantly different flow rates and operation mode. This was also observed experimentally, as devices required different back pressures to operate stably. Focus was thus shifted to the optimization of the deep etch fabrication process to increase the impedance without making use of the bead filling method. The dimensions of the latest generation emitters are presented in Table 1, which also includes the expected dimensions of the next generation devices. It is clear from the table that the present devices have a much lower impedance than the bead filled ones - so that they are not expected to operate in ionic mode - but that the upcoming generation will display both high impedance and low variability.

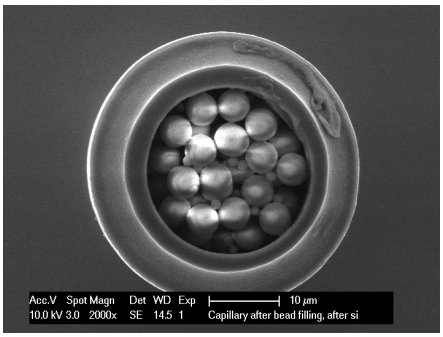

Figure 4. SEM image of $22\mu m$ inner diameter emitter from the 1^{st} generation filled with $5\mu m$ silicon dioxide beads.

Table 1. Effective inner diameter and corresponding hydraulic impedance of latest generations of electrospray emitters fabricated at EPFL. Values under parenthesis represent an estimation

Gen.	Beads	Status	L	(Effective) D (μm)			(Effective) R_{fl} ($kg\ s^{-1}\ m^{-4}$)			
				Min	Median	Max	Min	Median	Max	Variation
1.0	yes	Fabricated	100	(3.0)	(5.4)	(8.9)	(1.58e17)	(1.82e17)	(1.96e18)	(990%)
2.0	no	Fabricated	100	9.5	10.2	10.9	3.34e15	1.43e16	1.90e16	109%
3.0	no	Planned	50	4.5	5.0	5.5	3.93e16	1.24e17	1.89e17	120%

III. Fabrication

III.A. Emitter and extractor fabrication

The fabrication steps for the extractor wafers are shown in figure 5. The starting wafer has a 400 μm thick handle layer and a 50 μm thick device, with 2μm oxide insulation. A wet oxidation is done to provide a 2.2 μm hard mask (Figure 5a). The extractors are defined though standard photolithography and Deep Reactive Ion Etch (DRIE) processes (Figure 5b). The backside of the wafer is patterned in a second front-to-back aligned lithography to provide the opening in the extractor handle, with sufficient clearance for the emitted spray. The oxide of the hard masks and suspended membranes are then removed with a wet HF etch. A 2 μm PECVD oxide is then re-deposited on the extractor front side to improve electrical isolation with the emitter. Finally, a thin aluminum layer is deposited to connect the extractor device and handle layers (Figure 5c).

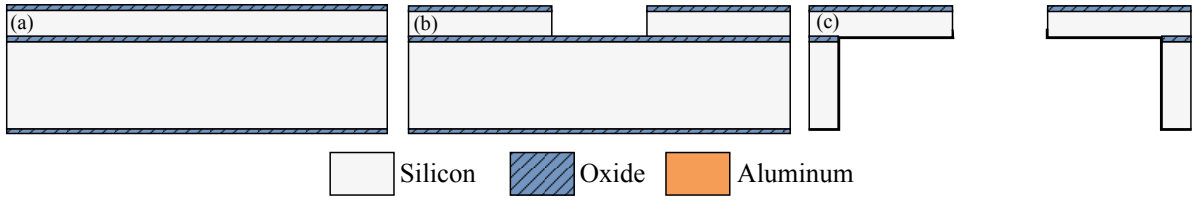

Figure 5. Fabrication steps for the extractor wafers. The SOI wafers have 50 μm thick device layer, 2 μm thick buried oxide layer and 400 μm thick handle layer.

The starting emitter wafer has a 400 μm handle and a 100 μm device, with again 2μm oxide insulation. A 2.2 μm oxide hard mask is again grown (Figure 6a). The critical lithography and etch defining the capillary inner diameter of the emitters are done first to ensure optimal conditions. The liquid feedthrough reservoir is then etched from the backside of the wafer in a two step process. First, an inner reservoir region is defined by etching the oxide hard mask. A thick resist (AZ9260) is then re-spun and patterned to define the reservoir outer dimensions (Figure 6b). The two-step reservoir is etched in a Silicon/Silicon dioxide/Silicon sequence. To pattern the exterior of the capillaries on the front side, a 15 μm dry film negative resist (DuPont MX5015) is laminated and patterned in a critical front-to-front alignment (Figure 6d). The tips of the capillaries are then sharpened with an isotropic silicon etch. Follows the silicon DRIE which defines the standoff height of the emitters (Figure 6e). The emitters are finally opened by a vapor phase HF release (Figure 6f). Future devices will also include the deposition of a thin MVD® coating to increase the hydrophobicity of the exterior of the emitters.

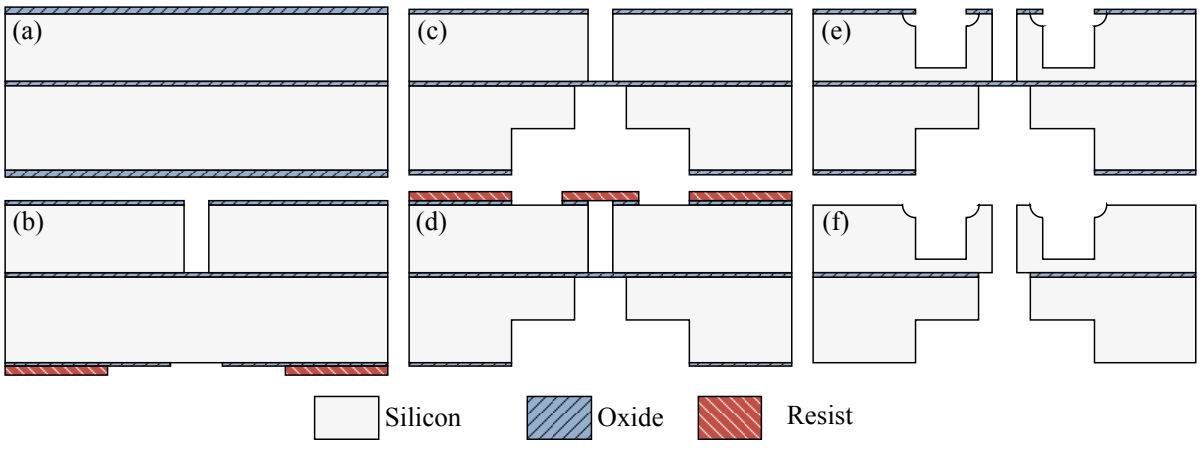

Figure 6. Fabrication steps for the emitter wafers. The SOI wafers have 100 μm thick device layer, 2 μm thick buried oxide layer, and 500 μm thick handle layer. The thermal oxide on both faces is 2.2 μm thick.

III.B. Wafer level assembly

The emitter and extractor wafers are bonded by thermo-compression with a laminated 50 μm dry film (DuPont MX5050) interface. The film is first applied to the extractor wafer and patterned to provide clearance for the spray and allow some deformation of the polymer during bonding (Figure 7a-b). Both wafers are aligned and pressed for 60 minutes at 115°, with a pressure load of 100 N/cm^2 (Figure 7c). The resulting bond provides high alignment accuracy, has high dielectric insulation (>3kV experimental) and can be reversed with an isopropanol or acetone soak for failure analysis. The stacks are finally diced with protective tape applied on both sides (Figure 7d).

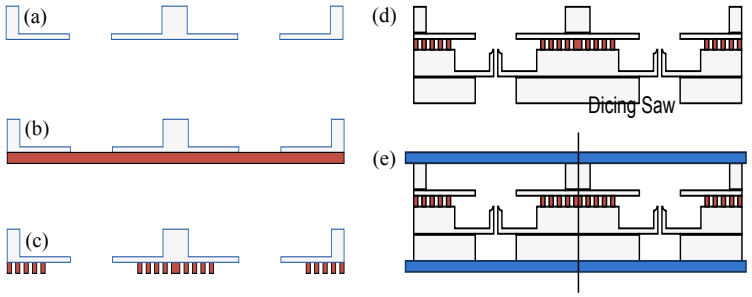

Figure 7. Process for the bonding and dicing of the emitter/extractor stacks.

IV. Experimental results

IV.A. Test setup

The basic test setup for thruster characterization is shown in Figure 8(a) and consists of two chambers. The main chamber holds the mounting interface to receive the test assembly, a modified Thorlabs lens cap (Figure 8(b)) that can be quickly exchanged. The second chamber holds the ionic liquid reservoir, kept under vacuum to avoid liquid contamination by ambient humidity. The liquid is itself transferred using a glass capillary by applying a pressure differential and dropped on the backside of the assembly, where capillarity transports it to the emitter tip. An EPDM rubber o-ring, clamped down in between the die and holder, prevents the ionic liquid from spilling out and creating short circuits. The basic setup sprays downwards, although alternate setups have been used to successfully spray sideways, indicating that gravity has little influence on the liquid feed.

For standard tests, the front clamping plate, connected to the extractor, is grounded while the lens cap is set to high voltage, either positive or negative. The current carried by the spray is collected by a Kimball physics Faraday cup and measured by a Keithley 6487 pico-ammeter. The current on the extractor and the high voltage source are also measured. The instruments are controlled a semi-automated Matlab routine and the current measurements recorded using a Texas Instruments NI-USB 4211 DAQ card.

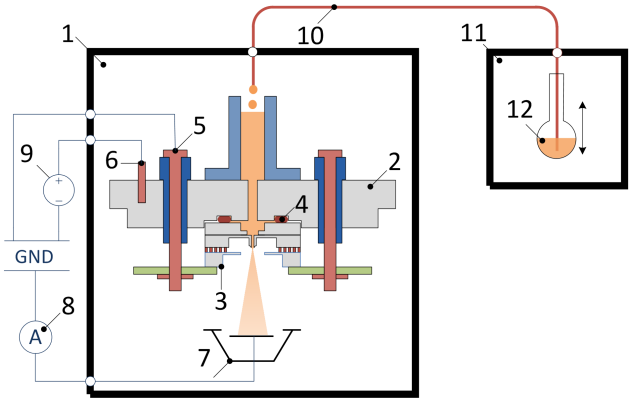

(a) Schematic of the test rig for thruster characterization. 1) Main chamber 2) Chip Holder 3) Thruster chip 4) O-Ring 5)Extractor addressing 6) Liquid addressing 7) Faraday cup 8) Pico-ammeter 9) High voltage source 10) Glass capillary 11) Liquid chamber 12) Liquid reservoir

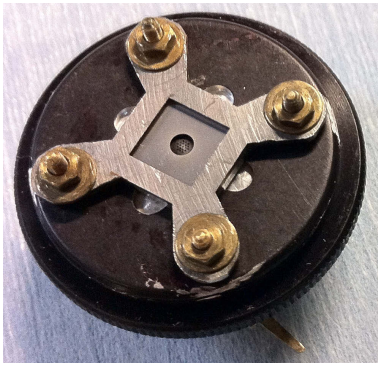

(b) Photograph of test assembly with 19x emitter array installed.

Figure 8. Setup and assembly for IV measurements.

IV.B. IV characteristics

In an initial characterization of the fabricated devices, IV curves can been traced for individual or arrays of emitters, both in unipolar and bi-polar operation. Figure **??** shows plots of a 19x emitter array composed of 10 μm inner diameter emitters with 200 μm diameter extractors. The current is swept up in 10 V steps from 500V to 1000V (Figure 9(a)), then swept down (Figure 9(b)). While some hysteresis is clearly seen between the two curves, the "onset" and "offset" voltages are both at approximately 825 Volts, with current values quickly reaching 2 μA. Very low leakage current was seen in this case, with almost no difference between the collected current (PAM current) and the source current.

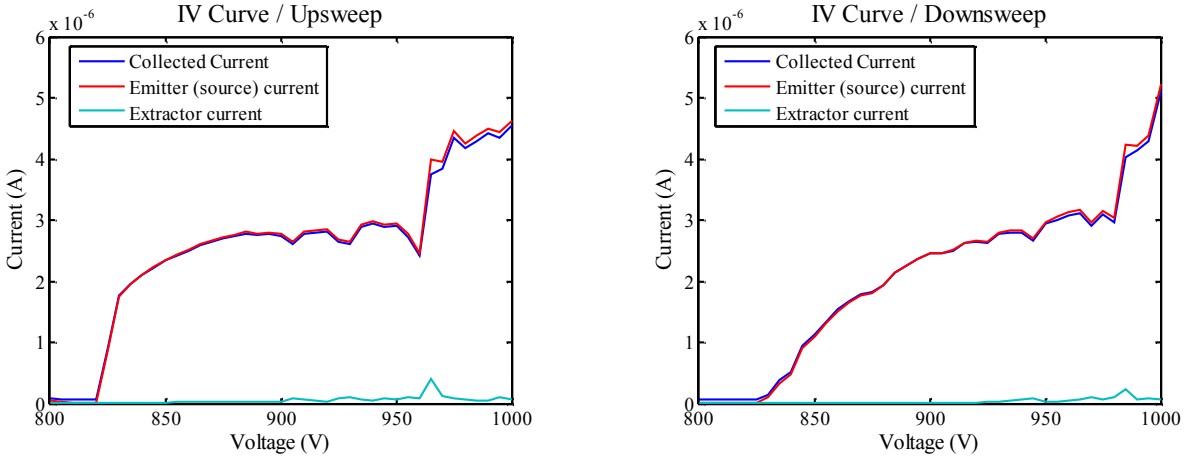

(a) Upsweep (b) Downsweep

Figure 9. Unipolar IV curves for a 19x emitter array, with 200μm diameter extractors. The voltage steps are of 10V and, in the case of bipolar operation, the switching frequency is 0.5 Hz.

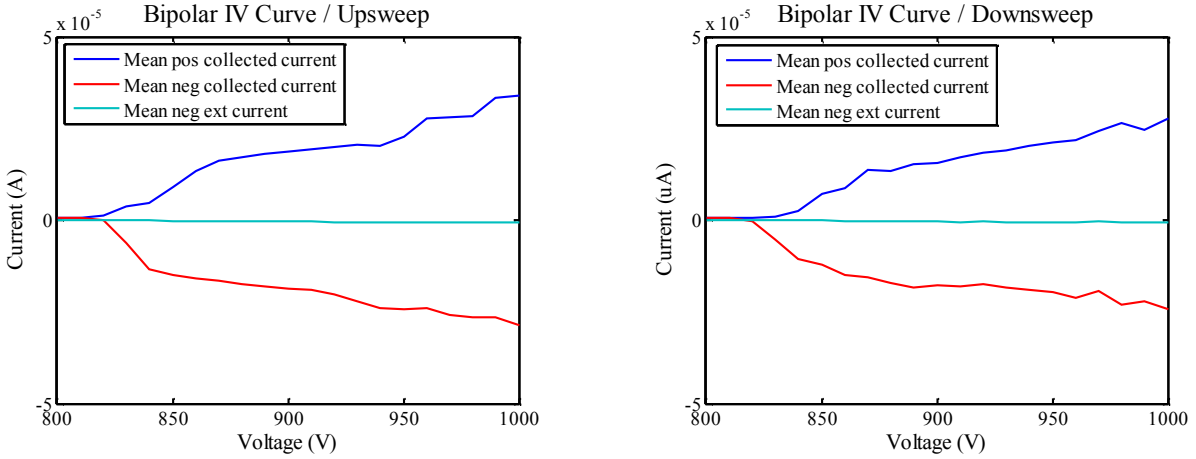

(a) Upsweep (b) Downsweep

Figure 10. Bipolar IV curves for a 19x emitter array, with 200μm diameter extractors. The voltage steps are of 10V and, in the case of bipolar operation, the switching frequency is 0.5 Hz.

The same device could be operated in bipolar mode (0.5 Hz frequency), with the alternated emission of positive and negative particles (Figure 10). The negatively charged spray initiated at lower voltage, which is consistent with the smaller mass of the BF_4^- anions. This device could be operated for several hours, but eventually failed from an apparent surface wetting probably due to a back flux of particles. Ionic liquid escaping the confinement of the capillary continues to be a life limiting factor, as it eventually leads to the electrical shorting of the emitter and extractor. The addition of the hydrophobic layer is believed instrumental to the resolution of this problem.

IV.C. Beam composition (Time-of-Flight)

Various Time-of-Flight (ToF) experiments were completed as part of the investigations. The experimental set-up for ToF data collection is the same as in Figure 8, except with the addition of a relatively simple electrostatic gate 10mm downstream from the emitter.[19] The gate is attached to a DEI PVX-4150 high speed switch, enabling the gate to switch from ground to emitter voltage in 20 nanoseconds. Also, rather than the Kimball physics Faraday cup illustrated in Figure 8, the plume is collected on a 70mm diameter flat plate situated up to 400mm downstream. This larger collection area allow for ToF to be collected without the use of a Einzel lens-like focussing device. A fine mesh is situated above the plate, to which is applied a negative potential difference to suppress secondary electron emission. The current collected is amplified by a Femto variable-gain high-speed current amplifier. The signal is then supplied to a Wavesurfer oscilloscope for analysis and collection. ToF analysis was completed for the 2nd generation devices, with on average a 10.2 μm inner diameter, as listed in Table 1.

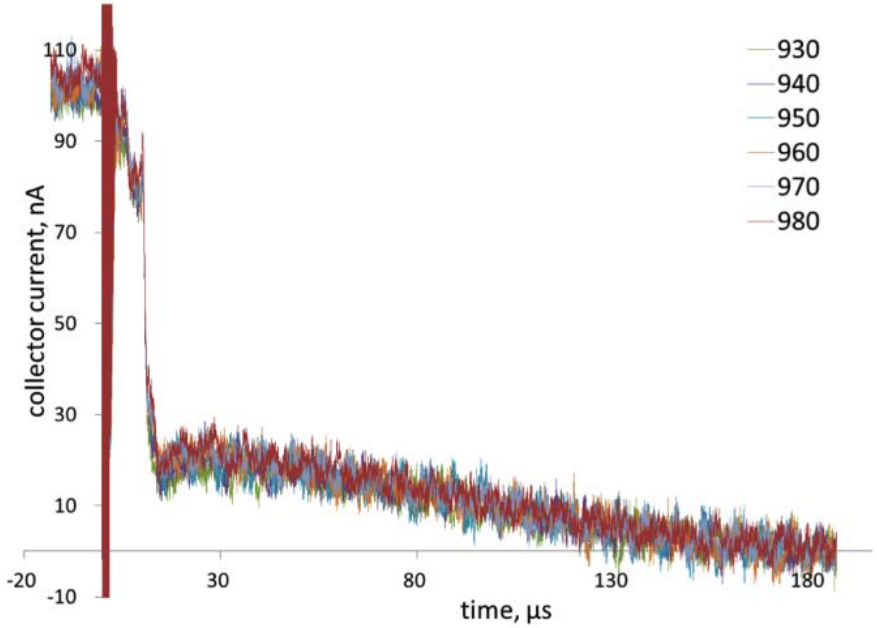

Figure 11. ToF traces with varying emitter voltage. In Unipolar mode. Monomer and dimer ions present, and tail of droplets

Figure 11 illustrates the time-of-flight traces for a positive emitter voltage polarity unipolar voltage sweep, similar to that shown in Figure 9(a). A mixture of ions and droplets is illustrated, with the ionic current dominating, but droplets still being present with a substantially different charge/mass ratio.

An approximate value of the thrust and specific impulse can be calculated from the Time-of-Flight data.[20] From Figure 11 the specific impulse is approximately 180s, with the emitter thrust being of the order of 0.5 μN.

ToF experiments were also completed in bipolar mode, with again the emitter voltage varied. The experiments were similar to the current voltage sweep illustrated in Figure 10. The ToF data for these bipolar emitter voltage-varying tests is illustrated in Figure 12, for negative and positive polarities respectively. The bipolar frequency of the particular experiment shown was 0.5Hz. The ToF traces all show a mixed mode of operation, dominated by the ionic current, as was the case for the experiments generally.

Figure 13 show the calculated approximate values of the thrust and specific impulse for the negative and positive polarities of the bipolar sweep respectively. Both polarities demonstrate a specific impulse of the order of 200s, and an emitter thrust of 0.3 - 0.8 μN. The polarity seems to have little effect on the plume composition, and also the specific impulse values are in agreement with the values found for unipolar mode.

The generally low specific impulse values indicate that, as expected, the latest fabricated devices have an hydraulic impedance too low to allow stable ionic mode operation. To improve the specific impulse requires the removal of the droplet component of the electrospray plume, which can be achieved by reducing the flow rate. In the past, we have experienced this situation either by using the high impedance, bead filled emitters, or by pressure feeding the propellant.[20] In the latter, instead of feeding the $EMI-BF_4$ propellant into the

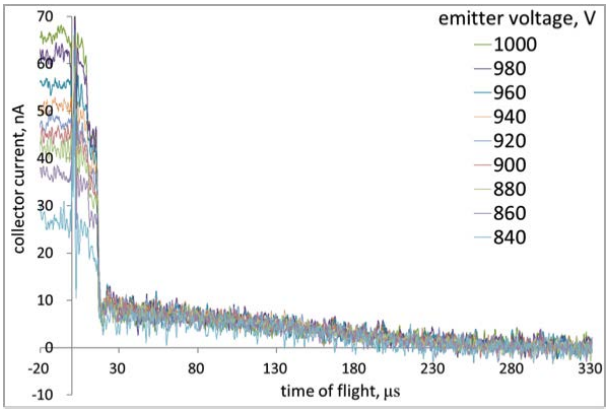

(a) Negative polarity

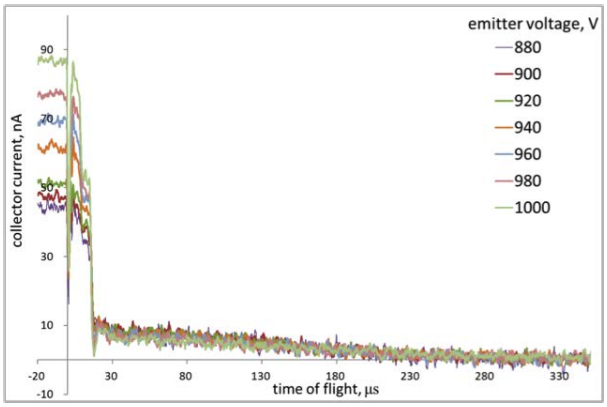

(b) Positive polarity

Figure 12. Variation of time-of-flight traces with emitter voltage in negative polarity for bipolar spraying. Completed at a bipolar frequency of 0.5Hz.

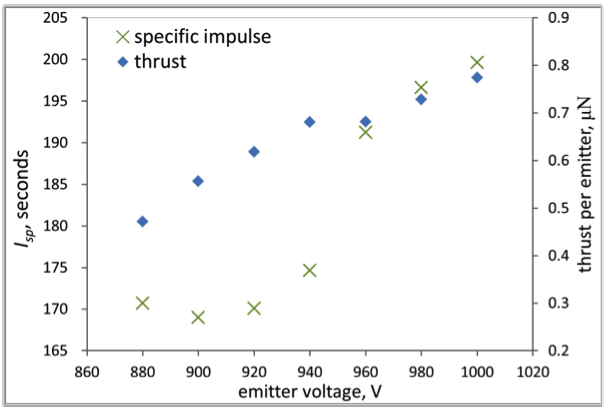

(a) Negative polarity

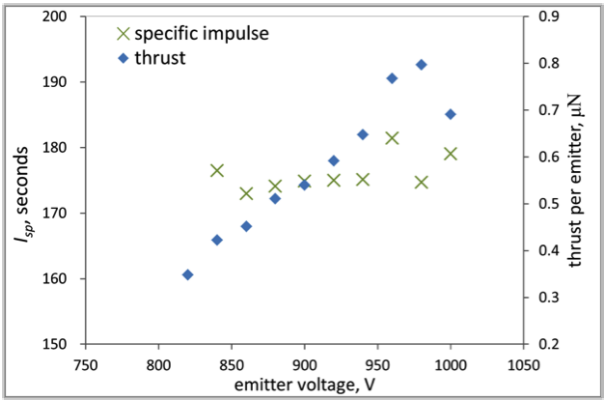

(b) Positive polarity

Figure 13. Variation of specific impulse and emitter thrust with emitter voltage, in negative polarity for bipolar spraying. Completed at a bipolar frequency of 0.5Hz.

thruster chip holder using droplets, the chip holder was directly attached to the capillary feed line and the pressure in the liquid chamber (no. 11 in Figure 8(a)) adjusted. It was found that this propellant feeding method was unreliable, with the initial 100mBar reservoir pressure often resulting in the uncontrollable flooding of the emitter and extractor surfaces. Therefore this "reservoir fed" method is currently not being used, but may be revisited with upcoming high impedance emitters.

Even with the current devices, though, recent tests have demonstrated that, in some conditions, a seemingly ionic mode could be reached. Indeed, long duration bipolar tests showed a switch after several hours of operation. Such ToF data is illustrated in Figure 14. Two ToF traces are shown, one after 1/2 an hour of operation, and the second after 4 and hours of operation. The data after a longer duration demonstrates an ionic mode of operation, with no (or at least very little) droplets present. The specific impulse for the two ToF trace are 190s and 2500s respectively. Interestingly the mode change was also accompanied by a change in the emitter current from 1200nA to 250nA, but the amount of collector current remains relatively constant. This suggest that ionic mode has a smaller plume half-angle, decreasing from 34 degrees in mixed mode (in approximate agreement with the data shown in Section IV. D. below), to 17 degrees in ionic mode. The reason for this change in mode remains unclear though. The emitter eventually failed after approximately 10 hours of spraying, due to an accumulation of liquid between the emitter and extractor. This accumulation of liquid may be the reason for the change in mode, with the electric field changing as the accumulation increased possibly resulting in a lower flow rate and therefore ionic mode.

In conclusion, substantial Time-of Flight data suggests that the current devices can emit sprays with a range of beam compositions, from mixed ion/droplets to nearly ionic. The operation is currently not well controlled, though; a situation which it is believed will be improved with the higher impedance third

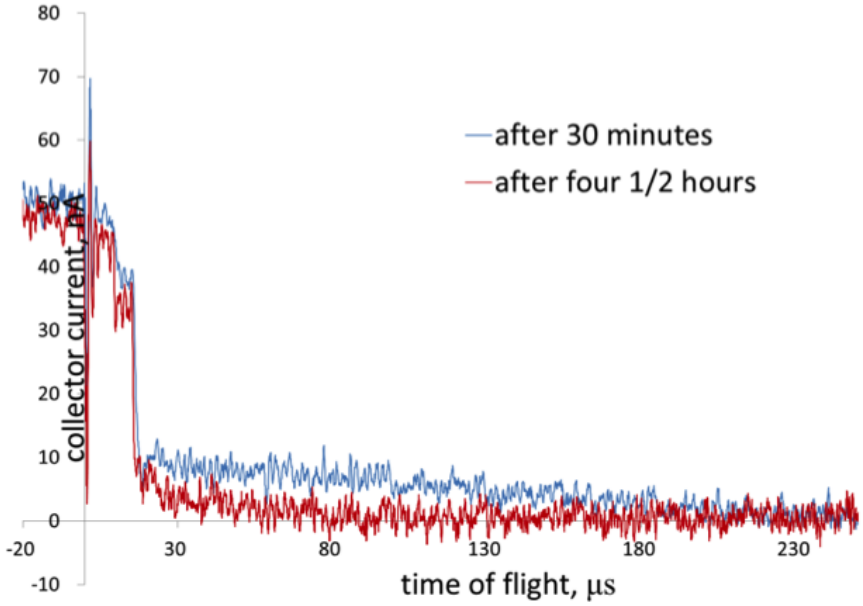

Figure 14. ToF traces with varying emitter voltage. In Unipolar mode. Monomer and dimer ions present, and tail of droplets

generation emitters described in Table 1.

IV.D. Beam shape

The shape and angle of the emitted beam are of great importance to the system performance of the thrusters. First, particle emission off the desired thrust direction will reduce the thrust to power efficiency of the system and result in propellant waste, reducing the achievable Δv of the system. Second, asymmetry or off-centering of the emitted beam would generate a lateral thrust vector and lead to spacecraft attitude control issues. Third, from the design point of view, the spray angle drives the minimum dimensions of the extractor and accelerator electrodes as well as the pitch between emitters, driving the packing density of arrays. For accelerator design, the divergence of the beam is also necessary as input to the beam shaping design and simulations.

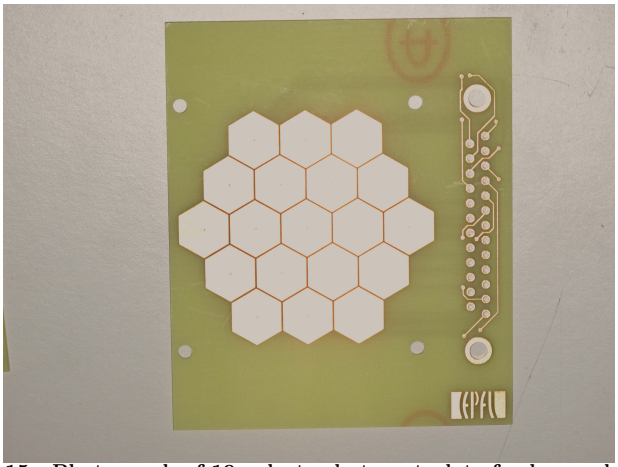

Figure 15. Photograph of 19x electrode target plate for beam shape analysis.

To characterize the beam shape and emission angle, a multiple electrode detector scheme has been implemented. In the first attempt, 19 hexagonal detector plates have been fabricated on a FR4 printed circuit board (PCB) as shown in Figure 15. Switching electronics have been built to switch through all plates sequentially during the spray process and record the spray current from the plates in bipolar spray conditions. So far, two devices have been characterized for beam shape and emission angle results with this

19-plate hexagonal configuration. Figure 16 shows the spray currents recorded in the 19-plate detectors as a function of the emission angle at two different emission voltages with both polarities. In Figure 17(a), a simple second order extrapolation of the current readings in 5 plates along the cross-section of the plates is used to estimate the beam emission angle as a function of the emission voltage. This shows that the emission angle, while starting with half-angles just under 20°, tends, for both polarities, to double as the voltage is increased. In Figure 17(b), the total spray currents recorded in the 19 plates as a function of emission voltage are plotted. The estimate of emission angle relies on only 5 data point along the cross section of emission. To improve the accuracy of beam angle measurement, a new 19-plate annular ring configuration has been built, using the same switching electronics. Tests on the beam shape with this configuration will be reported later.

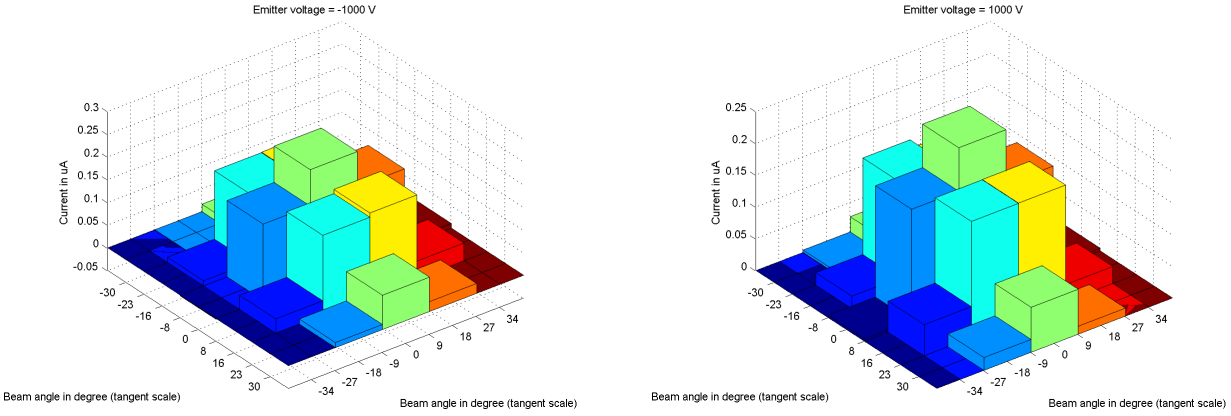

(a) Negative (-1000V) emission

(b) Positive (1000V) emission

Figure 16. Spray current at distribution across the detector plates as a function of spray angle for (a) -1000V emission voltage and (b) 1000V emission voltage.

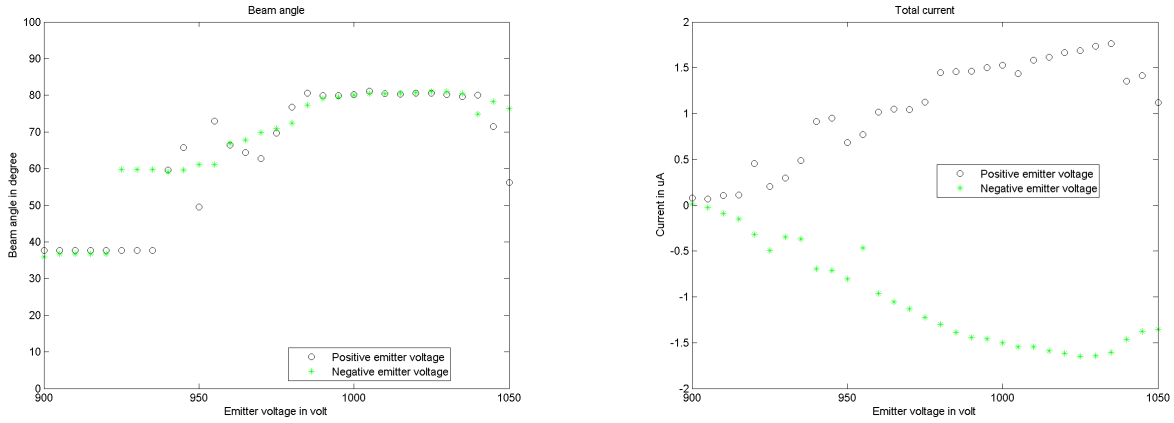

(a)

(b)

Figure 17. (a) An approximate estimation of the beam angle as a function of the emission voltage. (b) Total spay current as a function of the emission voltage.

V. Conclusion

We have shown our latest advances in the development of electrospray thrusters for small satellites. By operating in internally fed bi-polar mode, arrays of microfabricated emitters can to be integrated in a propulsion system suitable for micro and nano satellites. Specific impulses of several thousands have been observed and depend strongly on the operating conditions of the device - a particularity that can be utilized to allow tunable Thrust vs I_{sp} characteristics. High specific impulse remains difficult to attain stably, requiring the very low propellant flow rate associated with high hydraulic impedance capillaries. The method of silica micro bead filling previously used to achieve this high impedance was dismissed with focus turned to the optimization of the capillary etch process. Current devices have an impedance an order of magnitude below the bead filled ones, explaining their mixed mode operation, but are considerably more reproducible. Upcoming devices are expected to have impedances comparable to the bead filled capillaries while having high uniformity.

The full microfabrication process was presented, including a wafer-level assembly method using a thin laminated resist film.

Fabricated, "low impedance" devices were tested for their "turn-on"/"turn-off" voltages, beam composition and plume angle. Initial analysis shows slight hysteresis and asymmetry between the positive and negative extracted species. The composition, while mostly ionic, also still includes a significant fraction of droplets, effectively reducing the I_{sp} and efficiency of the spray, and highlighting the importance of the high impedance.

A new target plate setup was also introduced, used to map the beam shape in various operation mode. First results indicated beam half-angles in the range of 35-45°, although this angle is seen to be dependent on the operation voltage and beam composition.

Acknowledgments

This work has been supported by the MicroThrust project, grant agreement number 263035, funded by the EC Seventh Framework Programme theme FP7-SPACE-2010. The authors thank the project partners Nanospace, TNO, SystematIC, the Swiss Space Center and the staff of the CSEM cleanroom.

References

[1]Lopez Urdiales, J. M., *Progress in colloid propulsion*, Ph.D. thesis, MIT, 2004.

[2]Taylor, G., "Disintegration of water drops in an electric field," *Proceedings of the Royal Society of London*, Vol. 280, No. 1382, July 1964, pp. 383–397.

[3]Romero-Sanz, I., Bocanegra, R., and De La Mora, J. F., "Source of heavy molecular ions based on Taylor cones of ionic liquids operating in the pure ion evaporation regime," *Journal of Applied Physics*, Vol. 94, No. 5, 2003, pp. 3599.

[4]Krpoun, R., Räber, M., and Shea, H. R., "Microfabrication and test of an integrated colloid thruster," *21st International Conference on Micro Electro Mechanical Systems*, 2008, pp. 964–967.

[5]Krpoun, R. and Shea, H. R., "Integrated out-of-plane nanoelectrospray thruster arrays for spacecraft propulsion," *Journal of Micromechanics and Microengineering*, Vol. 19, No. 4, April 2009, pp. 045019.

[6]Lenguito, G., De La Mora, J. F., and Gomez, A., "Multiplexed Electrospray for Space Propulsion Applications," *46th AIAA/ASME/SAE/ASEE Joint Propulsion Conference and Exhibit*, No. July, 2010, pp. 1–11.

[7]Lenguito, G., De La Mora, J. F., and Gomez, A., "Design and Testing of Multiplexed Electrospray with Post-Acceleration for Space Propulsion Applications," *47th AIAA/ASME/SAE/ASEE Joint Propulsion Conference and Exhibit*, No. August, 2011, pp. 1–11.

[8]Ataman, C., Dandavino, S., and Shea, H., "Wafer-level Integrated Electrospray Emitters for a Pumpless Microthruster System Operation in High Efficiency Ion-Mode," *IEEE MEMS*, 2012.

[9]Lozano, P. C. and Martínez-Sánchez, M., "Ionic liquid ion sources: characterization of externally wetted emitters," *Journal of Colloid and Interface Science*, Vol. 282, No. 2, Feb. 2005, pp. 415–21.

[10]Courtney, D. G. and Lozano, P. C., "Development of Ionic Liquid Electrospray Thrusters using Porous Emitter Substrates," *International Conference on Space Technology and Science*, 2009, pp. 1–6.

[11]Legge Jr., R. S. and Lozano, P. C., "Electrospray Propulsion Based on Emitters Microfabricated in Porous Metals," *Journal of Propulsion and Power*, Vol. 27, No. 2, March 2011, pp. 485–495.

[12]Liaw, D. C., Gilchrist, B. E., and Liu, T. M., "Simulation of self-neutralization techniques for charged particle thrusters," *47th AIAA/ASME/SAE/ASEE Joint Propulsion Conference and Exhibit*, 2011, pp. 3184–3197.

[13]Krpoun, R., Smith, K. L., Stark, J. P. W., and Shea, H. R., "Tailoring the hydraulic impedance of out-of-plane micromachined electrospray sources with integrated electrodes," *Applied Physics Letters*, Vol. 94, No. 16, 2009, pp. 163502.

[14]Ergun, S., "Fluid flow through packed columns," *Chemical Engineering Progress*, Vol. 48, No. 2, 1952, pp. 89–94.

[15]Martino, W., De La Mora, J. F., Yoshida, Y., Saito, G., and J, "Surface tension measurements of highly conducting ionic liquids," *Green Chemistry*, Vol. 8, No. 4, 2006, pp. 390.

[16]Auwerda, G. and Kloosterman, J., "Comparison of experiments and calculations of void fraction distributions in randomly stacked pebble beds," *Advances in Recactor Physics to Power the Nuclear Renaissance*, 2010.

[17]Goodling, J., Vachon, R., Stelpflug, W., Ying, S., and Khader, M., "Radial porosity distribution in cylindrical beds packed with spheres," *Powder Technology*, Vol. 35, No. 1, May 1983, pp. 23–29.

[18]Thadani, M., "Variation of local void fraction in randomly packed beds of equal spheres," *Industrial Engineering Chemistry*, Vol. 5, No. 3, 1966.

[19]Dandavino, S., Ataman, C., Shea, H., Ryan, C., and Stark, J., "Microfabrication of Capillary Electrospray Emitters and ToF Characterization of the Emitted Beam," *32nd International Electric Propulsion Conference*, 2011, pp. 1–10.

[20]Ryan, C., Stark, J. P. W., Ataman, c., Dandavino, S., Chakraborty, S., and Shea, H., "MicroThrust MEMS electrospray emitters integrated microfabrication and test results," *AAAF-ESA-CNES Space Propulsion*, No. May, 2012.